Multiband theory of superconductivity at the $LaAlO_3/SrTiO_3$ interface

N. Mohanta[1,*] and A. Taraphder[1,2]

[1]*Department of Physics, Indian Institute of Technology Kharagpur, West Bengal 721302, India*

[2]*Centre for Theoretical Studies, Indian Institute of Technology Kharagpur, West Bengal 721302, India*

(Received 10 July 2015; revised manuscript received 3 October 2015; published 30 November 2015)

We present a multiband model for superconductivity at the metallic interface between insulating oxides $LaAlO_3$ and $SrTiO_3$ (001). Using a self-consistent Bogoliubov–de Gennes theory, formulated with the realistic bands at the interface, we investigate the spin-singlet and spin-triplet pairings in intraband and interband channels. We find that the Rashba and atomic spin-orbit interactions at the interface induce singlet pairing in the interband channel and triplet pairing in both the intraband and interband channels when the pairing amplitude in the singlet intraband channel is finite. The gate-voltage variation of superconductivity is resolved in different pairing channels, compared with experimental results, and found to match quite well. Interestingly, an enhancement of the superconducting transition temperature by external in-plane magnetic field is found, revealing the existence of a hidden superconducting state above the observed one. As the interface is known to possess a high level of inhomogeneity, we explore the role of nonmagnetic disorder incorporating thermal phase fluctuations by using a Monte Carlo method. We show that even after the transition to the nonsuperconducting phase, driven by temperature or magnetic field, the interface possesses localized Cooper pairs whose signature was observed in previous experiments.

DOI: 10.1103/PhysRevB.92.174531 PACS number(s): 74.78.−w, 74.20.Rp, 74.40.−n, 61.43.Bn

I. INTRODUCTION

The discovery of superconductivity ($T_c \simeq 200$ mK) at the interface [1,2] between perovskite band insulators $LaAlO_3$ (LAO) and $SrTiO_3$ (STO) triggered a plethora of investigations [3–13] in the last few years due to its exotic nature arising primarily from the presence of competing ferromagnetism ($T_{\text{Curie}} \simeq 200$ K) [14–16], spin-orbit interaction (SOI) [17,18], and disorder [19–21]. In addition, the quasi-two-dimensional electron gas (q2DEG) at the interface [22] exhibits intriguing novel properties such as metal-insulator transition [23–27] and ferroelectricity [28]. On top of that, the ability to control these properties by an external electric field [29,30] added an extra dimension to the nanoelectronics industry [31,32].

The q2DEG is formed by an electronic transfer mechanism in which half an electronic charge per unit cell is transferred to the interface to avoid a polar discontinuity [33,34]. The electrons are confined in a few TiO_2 layers located within a region of about 10 nm thickness at the interface and occupy the t_{2g} orbitals of Ti ions [35,36]. Density functional theory (DFT) reveals that the d_{xy} band is situated below the d_{yz} and d_{zx} bands by ∼0.4 eV due to the confinement at the interface [37,38]. The spin degeneracy of the bands is lifted by the inversion symmetry-breaking Rashba SOI and an atomic SOI [39,40]. Magnetotransport measurements infer the presence of two types of carriers with different mobilities, and the high-mobility carriers have been predicted to be responsible for superconductivity [41–43]. Michaeli *et al.* [3] suggested that the system hosts the antagonistic ferromagnetic and superconducting orders by favoring a disorder-stabilized helical Fulde-Ferrell-Larkin-Ovchinnikov (FFLO) state induced by strong Rashba SOI. The complex nature of the coexisting phases [14,15,44] has naturally led to the predictions of unconventional superconductivity [45] and different magnetic ground states. The microscopic understanding of the origin of superconductivity remained obscure until the recent convincing evidence of electron-phonon coupling obtained using tunneling spectroscopy [46]. The LO phonons of STO were proposed to be responsible for mediating superconductivity in bulk STO [47]. Recent studies also show that the LO phonons of STO and the optical phonons at the interface can make a significant contribution to the interface superconductivity [11]. It is therefore apparent that phonons play the dominant role in electron pairing in other STO-based superconductors such as doped STO [48] and X/STO ($X = LaTiO_3$ [49], $GdTiO_3$ [50], FeSe [51]) interfaces. The superconductivity at the LAO/STO interface is unique in the following aspects: (i) It appears at very low carrier concentrations ($\sim 10^{-13}$ cm^{-2}) [29]. (ii) The transition temperature (T_c) shows Berezinsky-Kosterlitz-Thouless (BKT)-like behavior [29] while the pairing gap or the superfluid density follows BCS prediction: $2\Delta_0/(k_B T_g) \simeq 3.4$, where Δ_0 is the pairing gap at $T = 0$, k_B is the Boltzmann constant, and T_g is the so-called gap-closing temperature [52]. (iii) It coexists with inhomogeneous ferromagnetic puddles of large moments ($\sim 0.4\mu_B$ per interface unit cell) [14]. The coexistence of the competing orders, albeit in phase-segregated regions [4,5,44], gives rise to fascinating phenomena such as the enhancement of superconductivity by magnetic field [53] and the magnetic-field-assisted transient superconductivity [54], leading to a possible "hidden order." However, despite intensive previous studies, complete theoretical understanding of the nature of the multiband superconductivity is lacking and necessitates a careful and thorough theoretical analysis.

In the following, we use a three-orbital model for superconductivity to develop an understanding of the nature of superconductivity at the interface in the presence of magnetic moments and try to shed light on the questions raised above. We study the spin-singlet and spin-triplet electron pairing in intraband and interband channels. Using a self-consistent Bogoliubov–de Gennes (BdG) method, formulated with the realistic bands at the interface, we explore the mean-field phase

*nmohanta@phy.iitkgp.ernet.in

diagrams, the role of spin-orbit interactions, and the effect of external magnetic field on the electron pairing. It is found that the pairings in the singlet interband channel and triplet intraband and interband channels are induced by the Rashba and atomic SOIs when the pairing amplitude in the singlet intraband channel is finite. Taking a cue from the experimental data, we incorporate the gate voltage in our analysis, study the gate-voltage variation of the pairing amplitudes, and plot the phase diagram to compare with the experimental results. We study the behavior of the pairing amplitudes in the presence of an external in-plane magnetic field and find an enhancement of the superconducting transition temperature when the magnetic field is applied along certain directions in the interface plane. The magnetic field enhancement of superconductivity has been observed experimentally [53] and arises because of the interplay between superconductivity and the competing ferromagnetism. It suggests a hidden superconducting phase above the superconducting transition temperature. Since the interface superconductivity is highly inhomogeneous in nature and appears at very low carrier concentration, the thermal phase-fluctuation becomes significant. We study the phase transition from a superconducting to a nonsuperconducting state, driven by temperature or perpendicular magnetic field, taking into account the thermal phase fluctuation using a Monte Carlo method, and observe that there are localized Cooper pairs in the nonsuperconducting phase. The presence of these localized Cooper pairs has been confirmed in a previous experiment [55].

The remainder of this paper is organized as follows. In Sec. II, we discuss the origin of ferromagnetism and superconductivity and introduce the multiorbital effective Hamiltonian for the interface q2DEG. In Sec. III, we formulate the self-consistent equations for the superconducting order parameters within the multiorbital BdG framework. In Sec. IV, we present and discuss our results obtained within the self-consistent BdG method. In Sec. V, we present a Monte Carlo analysis of the thermal phase fluctuation in superconductivity. The conclusions are briefly summarized in Sec. VI.

II. EFFECTIVE THREE-ORBITAL MODEL OF SUPERCONDUCTIVITY

In the following, we elaborate on the microscopic mechanisms of ferromagnetism, superconductivity, and other ingredients of the interface q2DEG and establish the effective Hamiltonian for the interface electrons.

The electrons coming from the top $LaAlO_3$ layer to neutralize the polarization discontinuity at the interface predominantly occupy the d_{xy} orbitals of Ti ions in the terminating TiO_2 layer and establish quarter-filled d_{xy} states. Because of large on-site Hubbard and nearest-neighbor Coulomb repulsive interactions at the interface, all the electrons get localized at the interface sites and form a charge-ordered insulating ground state with a weak antiferromagnetic superexchange coupling mediated via the oxygen atoms [3,56]. Additional electrons, supplied by the application of the back-gate voltage or the oxygen vacancies near the interface, will find the top TiO_2 layer energetically unfavorable and go to the next TiO_2 layer to occupy the t_{2g} orbitals of Ti ions. The electrons in the t_{2g} orbitals in the next TiO_2 layer participate in conduction

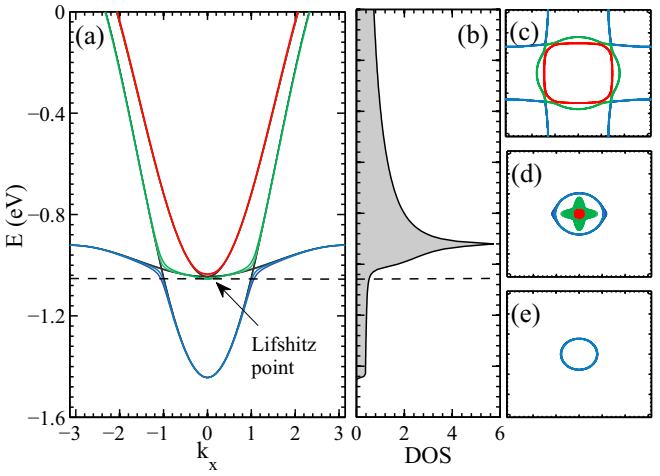

FIG. 1. (Color online) (a) The band structure of the three t_{2g} orbitals in the presence of the Rashba and atomic SOIs (spectrum of $\mathcal{H}_0 + \mathcal{H}_{\rm ASO} + \mathcal{H}_{\rm RSO}$). The spin-orbit interactions result in mixing of the original bands (plotted by black lines). The dashed horizontal line, at $\mu \simeq -1.04$ eV, denotes a Lifshitz transition point at which the two upper bands start getting occupied. (b) the total density of states as a function of energy. The Lifshitz transition is reflected by the sharp jump in the density of states near the transition point. The change in the Fermi-surface topology at energy (c) below, (d) near, and (e) above the Lifshitz transition.

and exhibit superconductivity. Spectroscopic experiments [43] and DFT studies [39,40] show that, due to confinement at the interface, the d_{xy} band is lower in energy at the Γ point by $\sim$0.4 eV than the quasi-one-dimensional, relatively heavier d_{yz}, d_{zx} bands. When the Fermi level is tuned, the system encounters a Lifshitz transition at an electron concentration $n_c \simeq 1.68 \times 10^{13}$ cm^{-2}, where the low-mobility d_{yz}, d_{zx} electrons start getting occupied [43], as depicted in Fig. 1. An interesting feature of the band structure is that because of the atomic SOI, the orbital characters of the d_{xy} band and the heavier d_{yz}, d_{zx} bands get interchanged near the Lifshitz point, and the splitting due to Rashba SOI is significant only near the degeneracy points. The spin degeneracy in all the bands is lifted by the spin-orbit interactions, with the splitting being largest near the band-mixing points.

The wave functions of the itinerant electrons in the t_{2g} orbitals in the TiO_2 layer below the interface are extended to the terminating TiO_2 layer. Therefore, these electrons interact via a ferromagnetic exchange with the localized moments, leading to the in-plane ferromagnetic order. The exchange interaction can be described by a Hamiltonian $\mathcal{H}_{\rm FM} = \sum_i \sum_\alpha \int d\mathbf{r} J_\alpha \hat{\mathbf{S}}(\mathbf{R}_i) \cdot \hat{\mathbf{s}}_\alpha(\mathbf{r}) \delta(\mathbf{r} - \mathbf{R}_i)$, where $\hat{\mathbf{S}}(\mathbf{R}_i)$ is the spin operator at the local moment sites $\mathbf{R}_i$, $\hat{\mathbf{s}}_\alpha(\mathbf{r})$ is the spin-density operator in the itinerant orbital α (d_{xy},d_{yz},d_{zx}), and J_α is the strength of the exchange interaction. Since the itinerant d_{yz}, d_{zx} orbitals are orthogonal to the localized d_{xy} orbital, $J_{d_{xy}} \gg J_{d_{yz},d_{zx}}$ [3]. This is in agreement with the spectroscopic studies which indicate the d_{xy} nature of the in-plane ferromagnetism [57]. When treated at the mean-field level, $\mathcal{H}_{\rm FM}$ will essentially be reduced to $\mathcal{H}_{\rm FM} = \sum_{k,\alpha,\sigma,\sigma'} (h_{x\alpha}\sigma_x)_{\sigma,\sigma'} c^\dagger_{k\alpha\sigma} c_{k\alpha\sigma'}$, where $h_{x\alpha}$ are the Zeeman splitting amplitudes, corresponding to different orbitals of index α, along the in-plane direction

(taken to be along the x axis) with $h_{x\alpha} = h_{x1}$ for the d_{xy} orbital and $h_{x\alpha} = h_{x2}$ for the d_{yz}, d_{zx} orbitals ($h_{x1} > h_{x2}$). The attractive interaction, mediated by electron-phonon coupling, for the three itinerant orbitals can be expressed as $\mathcal{H}_{\rm SC} = -g\sum_{k,k',\alpha,\beta} c^\dagger_{k\alpha\uparrow} c^\dagger_{-k\beta\downarrow} c_{-k'\beta\downarrow} c_{k'\alpha\uparrow}$, where g is the strength of the pairwise electron-electron interaction and α, β are general running indices, each taking three values to designate the three orbitals. The spin-singlet and spin-triplet pairing amplitudes in the intraband and interband channels can be defined as $\Delta^s_{\alpha\beta} = -g\langle c_{k\alpha\uparrow} c_{-k\beta\downarrow}\rangle$ and $\Delta^t_{\alpha\beta\sigma\sigma} = -g\langle c_{k\alpha\sigma} c_{-k\beta\sigma}\rangle$, respectively. Neglecting fluctuations beyond mean field, the pairing term becomes $\mathcal{H}_{\rm SC} = \sum_{k,\alpha,\beta}(\Delta^s_{\alpha\beta} c^\dagger_{k\alpha\uparrow} c^\dagger_{-k\beta\downarrow} + \Delta^t_{\alpha\beta\uparrow\uparrow} c^\dagger_{k\alpha\uparrow} c^\dagger_{-k\beta\uparrow} + \Delta^t_{\alpha\beta\downarrow\downarrow} c^\dagger_{k\alpha\downarrow} c^\dagger_{-k\beta\downarrow} + \text{H.c.})$. We have $\Delta^t_{\alpha\beta\uparrow\uparrow} = \Delta^t_{\alpha\beta\downarrow\downarrow}$, and the orbitals are designated according to $(a,b,c) = (d_{xy}, d_{yz}, d_{zx})$ for notational convenience, where α, β now run over a, b, c.

Another significant feature of the interface q2DEG is the presence of the atomic and Rashba SOIs, which reorganize the spin and orbital degrees of freedom of the t_{2g} electrons. The atomic SOI, described by the Hamiltonian $\mathcal{H}_{\rm ASO} = \Delta_{\rm so}\vec{l}\cdot\vec{s}$, appears because of the crystal-field splitting of the atomic orbitals. In the t_{2g} orbital basis $(c_{ka\uparrow}, c_{kb\uparrow}, c_{kc\uparrow}, c_{ka\downarrow}, c_{kb\downarrow}, c_{kc\downarrow})$, $\mathcal{H}_{\rm ASO}$ can be written as [39]

$$\mathcal{H}_{\rm ASO} = \frac{\Delta_{\rm so}}{2}\sum_k (c^\dagger_{ka\uparrow}\ c^\dagger_{kb\uparrow}\ c^\dagger_{kc\uparrow}\ c^\dagger_{ka\downarrow}\ c^\dagger_{kb\downarrow}\ c^\dagger_{kc\downarrow}) \times \begin{pmatrix} 0 & 0 & 0 & 0 & 1 & -i \\ 0 & 0 & i & -1 & 0 & 0 \\ 0 & -i & 0 & i & 0 & 0 \\ 0 & -1 & -i & 0 & 0 & 0 \\ 1 & 0 & 0 & 0 & 0 & -i \\ i & 0 & 0 & 0 & i & 0 \end{pmatrix} \begin{pmatrix} c_{ka\uparrow} \\ c_{kb\uparrow} \\ c_{kc\uparrow} \\ c_{ka\downarrow} \\ c_{kb\downarrow} \\ c_{kc\downarrow} \end{pmatrix}, \quad (1)$$

where $\Delta_{\rm so} = 19.3$ meV is the strength of the atomic SOI. On the other hand, the Rashba SOI, which describes the broken inversion symmetry at the interface, is given by the following Hamiltonian:

$$\mathcal{H}_{\rm RSO} = \gamma\sum_{k,\sigma}(c^\dagger_{ka\sigma}\ c^\dagger_{kb\sigma}\ c^\dagger_{kc\sigma}) \times \begin{pmatrix} 0 & -2i\sin k_x & -2i\sin k_y \\ 2i\sin k_x & 0 & 0 \\ 2i\sin k_y & 0 & 0 \end{pmatrix} \begin{pmatrix} c_{ka\sigma} \\ c_{kb\sigma} \\ c_{kc\sigma} \end{pmatrix}, \quad (2)$$

where $\gamma = 20$ meV is the strength of the Rashba SOI. It is interesting to note that the Rashba SOI, in Eq. (2), is different from the usual form $\mathcal{H}'_{\rm RSO} = (\gamma/\hbar)(\vec{\sigma}\times\vec{p})\cdot\hat{z}$, which is observed in the 2DEG at semiconducting heterointerfaces. The $\mathcal{H}'_{\rm RSO}$ lifts the spin degeneracy everywhere in the Brillouin zone except the Γ point, and on the other hand, $\mathcal{H}_{\rm RSO}$ is purely multiband in nature [39]. Any anisotropy in the Rashba SOI [58] can bring nontrivial anisotropy in the electronic properties of the 2DEG.

The oxygen vacancies, which are developed at the interface during the deposition process, are considered as indispensable parts of the interface q2DEG and have a very significant role in ferromagnetism, superconductivity, and their coexistence [4,5]. We model these nonmagnetic impurities as the local random shifts in the chemical potential and express them by the Hamiltonian $\mathcal{H}_{\rm dis} = \sum_{i_d}^{N_d}\sum_{\alpha\sigma} V^{i_d} c^\dagger_{i_d\alpha\sigma} c_{i_d\alpha\sigma}$, where i_d denotes the defect sites with total number N_d, V^{i_d} is a random potential which varies within a range $[-W, W]$, and W is the strength of the disorder. The percentage of defect concentration is given by $n_d = N_d/N^2 \times 100$.

The total effective Hamiltonian for the interface electrons is therefore given by

$$\mathcal{H}_{\rm eff} = \mathcal{H}_0 + \mathcal{H}_{\rm ASO} + \mathcal{H}_{\rm RSO} + \mathcal{H}_{\rm FM} + \mathcal{H}_{\rm SC} + \mathcal{H}_{\rm dis}, \quad (3)$$

where $\mathcal{H}_0 = \sum_{k,\alpha,\sigma}(\epsilon_{k\alpha} - \mu) c^\dagger_{k\alpha\sigma} c_{k\alpha\sigma}$ describes the band dispersion of the electrons in the three t_{2g} orbitals with $\epsilon_{ka} = -2t_1(\cos k_x + \cos k_y) - t_2 - 4t_3\cos k_x\cos k_y$, $\epsilon_{kb} = -t_1(1 + 2\cos k_y) - 2t_2\cos k_x - 2t_3\cos k_y$, $\epsilon_{kc} = -t_1(1 + 2\cos k_x) - 2t_2\cos k_y - 2t_3\cos k_x$; μ is the chemical potential; and $t_1 = 0.277$ eV, $t_2 = 0.031$ eV, $t_3 = 0.076$ eV are the tight-binding parameters [39].

Although multiband superconductivity in this interface q2DEG was proposed previously [7,59], the explicit nature of the pairing symmetry and the intraband or interband superconductivity were not explored. Our model uses the realistic band structures, obtained from DFT studies [39], and treats the electron pairing in intraband and interband channels within the multiband BdG theory, which will be described below.

III. MULTIBAND BdG THEORY

The self-consistent BdG theory is perhaps the best available numerical technique to study the interplay of superconductivity with real-space inhomogeneity or competing orders such as ferromagnetism or a charge-density wave within the mean-field approximation in any experimentally realizable geometry. To begin with, the Hamiltonian $\mathcal{H}_{\rm eff}$ in Eq. (3) is written in the real lattice as

$$\begin{aligned}\mathcal{H}_{\rm BdG} = &-\sum_{ij,\alpha,\beta,\sigma,\sigma'}\left(t^{ij\sigma\sigma'}_{\alpha\beta} c^\dagger_{i\alpha\sigma} c_{j\beta\sigma'} + \text{H.c.}\right) \\ &-\sum_{i,\alpha,\sigma}\left(\mu - V^{i_d}\delta_{ii_d}\right) c^\dagger_{i\alpha\sigma} c_{i\alpha\sigma} \\ &+\sum_{i,\alpha,\sigma,\sigma'}(h_{x\alpha}\sigma_x)_{\sigma\sigma'} c^\dagger_{i\alpha\sigma} c_{i\alpha\sigma'} \\ &+\sum_{i,\alpha,\beta}\left(\Delta^s_{\alpha\beta}(r_i) c^\dagger_{i\alpha\uparrow} c^\dagger_{i\beta\downarrow} + \text{H.c.}\right) \\ &+\sum_{\langle ij\rangle,\alpha,\beta,\sigma}\left(\Delta^t_{\alpha\beta\sigma\sigma}(r_i) c^\dagger_{i\alpha\sigma} c^\dagger_{j\beta\sigma} + \text{H.c.}\right), \end{aligned} \quad (4)$$

where $t^{ij\sigma\sigma'}_{\alpha\beta}$ is the tight-binding hopping amplitude which contains $\mathcal{H}_0$, $\mathcal{H}_{\rm ASO}$, and $\mathcal{H}_{\rm RSO}$; $\Delta^{si}_{\alpha\beta} = -g\langle c_{i\alpha\uparrow} c_{i\beta\downarrow}\rangle$ and $\Delta^{ti}_{\alpha\beta\sigma\sigma} = -g\langle c_{i\alpha\sigma} c_{i\beta\sigma}\rangle$ are the local singlet and triplet pairing gaps; and δ_{ii_d} is Kronecker's delta function.

The Hamiltonian $\mathcal{H}_{\rm BdG}$ in Eq. (4) is diagonalized by the unitary Bogoliubov transformation $\hat{c}_{i\alpha\sigma} = \sum_{n,\sigma'} u^{i\sigma'}_{n\alpha\sigma}\hat{\gamma}^{\sigma'}_n + v^{i\sigma'*}_{n\alpha\sigma}\hat{\gamma}^{\sigma'\dagger}_n$, which yields the multiband BdG equations (σ', being

a dummy index, is omitted hereafter)

$$\sum_j \begin{pmatrix} \sum_\beta \Gamma^{ij\uparrow\uparrow}_{\alpha\beta} & \sum_\beta \Gamma^{ij\uparrow\downarrow}_{\alpha\beta} & \Delta^{tij}_{\alpha\beta\uparrow\uparrow}\delta_{\alpha\beta} & \Delta^{sij}_{\alpha\beta}\delta_{\alpha\beta} \\ \sum_\beta \Gamma^{ij\downarrow\uparrow}_{\alpha\beta} & \sum_\beta \Gamma^{ij\downarrow\downarrow}_{\alpha\beta} & -\Delta^{sij}_{\alpha\beta}\delta_{\alpha\beta} & \Delta^{tij}_{\alpha\beta\downarrow\downarrow}\delta_{\alpha\beta} \\ \Delta^{tij*}_{\alpha\beta\uparrow\uparrow}\delta_{\alpha\beta} & -\Delta^{sij*}_{\alpha\beta}\delta_{\alpha\beta} & -\sum_\beta \Gamma^{ij\uparrow\uparrow*}_{\alpha\beta} & -\sum_\beta \Gamma^{ij\uparrow\downarrow*}_{\alpha\beta} \\ \Delta^{sij*}_{\alpha\beta}\delta_{\alpha\beta} & \Delta^{tij*}_{\alpha\beta\downarrow\downarrow}\delta_{\alpha\beta} & -\sum_\beta \Gamma^{ij\downarrow\uparrow*}_{\alpha\beta} & -\sum_\beta \Gamma^{ij\downarrow\downarrow*}_{\alpha\beta} \end{pmatrix} \times \begin{pmatrix} u^j_{n\alpha\uparrow} \\ u^j_{n\alpha\downarrow} \\ v^j_{n\alpha\uparrow} \\ v^j_{n\alpha\downarrow} \end{pmatrix} = E_n \begin{pmatrix} u^j_{n\alpha\uparrow} \\ u^j_{n\alpha\downarrow} \\ v^j_{n\alpha\uparrow} \\ v^j_{n\alpha\downarrow} \end{pmatrix}, \tag{5}$$

where $\Gamma^{ij\sigma\sigma'}_{\alpha\beta} = -t^{ij\sigma\sigma'}_{\alpha\beta} - [(\mu - V^{i_d}\delta_{ii_d})\delta_{\sigma\sigma'} - (h_{x\alpha}\sigma_x)_{\sigma\sigma'}]\delta_{ij}\delta_{\alpha\beta}$. For a square lattice of size $N \times N$, the BdG Hamiltonian matrix has dimensions $12N^2 \times 12N^2$ for three orbitals. Using the above Bogoliubov transformation, the local pairing gaps can be obtained as

$$\begin{aligned} \Delta^{si}_{\alpha\beta} &= -\frac{g}{2}\sum_n \left[u^i_{n\alpha\uparrow} v^{i*}_{n\beta\downarrow} - u^i_{n\alpha\downarrow} v^{i*}_{n\beta\uparrow}\right] \tanh\left(\frac{E_n}{2k_BT}\right), \\ \Delta^{ti}_{\alpha\beta\sigma\sigma} &= -\frac{g}{2}\sum_{n,\langle j\rangle} \left[u^i_{n\alpha\sigma} v^{j*}_{n\beta\sigma} - u^i_{n\alpha\sigma} v^{j*}_{n\beta\sigma}\right] \tanh\left(\frac{E_n}{2k_BT}\right), \end{aligned} \tag{6}$$

where k_B is the Boltzmann constant and T is the temperature. The total occupation number $n = (1/N^2)\sum_{i,\alpha,\sigma} \langle c^\dagger_{i\alpha\sigma} c_{i\alpha\sigma}\rangle$ is computed using the following relation:

$$n = \frac{1}{N^2}\sum_{n,i,\alpha,\sigma} \left\{ \left|u^i_{n\alpha\sigma}\right|^2 f(E_n) + \left|v^i_{n\alpha\sigma}\right|^2 [1 - f(E_n)] \right\}, \tag{7}$$

where $f(E_n) = 1/[1 + \exp(E_n/k_BT)]$ is the Fermi function. In what follows, the BdG equations (5) are solved numerically on a square lattice with periodic boundary conditions to find the eigenvalues E_n and the local quasiparticle amplitudes $u^i_{n\alpha\sigma}$, $v^i_{n\alpha\sigma}$, and the new pairing gaps are calculated using Eq. (6). This process is repeated until self-consistency is reached at every lattice site. Finally, the average values are obtained via $\Delta^{s/t}_{\alpha\beta} = (1/N)\sum_i \Delta^{(s/t)i}_{\alpha\beta}$.

It is important to mention here that static mean-field theory neglects fluctuations and therefore overestimates the field amplitudes. The temperature and the magnetic field, being treated in the analysis, therefore should be seen as just parameters, and their qualitative features, not quantitative estimates, are relevant.

IV. RESULTS

Having formulated the self-consistent BdG theory, we now present the numerical results obtained on a 25×25 square lattice. First, we analyze, in the homogeneous situation ($n_d = 0$), the effects of Rashba and atomic SOIs on superconductivity, the gap structures, and the phase diagrams of the singlet and triplet pairings and then the effects of in-plane magnetic field on superconductivity.

Spin-orbit interactions are known to have unusual effects on superconductivity [60,61]. The gate-tunable Rashba SOI makes the interface q2DEG a potential candidate for spintronic applications [62] as well as a playground for the search for

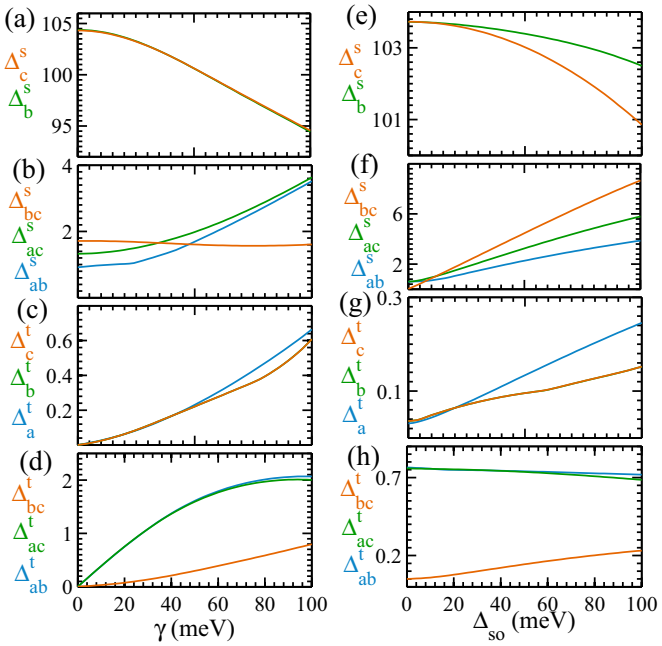

FIG. 2. (Color online) The variation of the singlet and triplet pairing amplitudes (in meV), in intraband and interband channels, with respect to the Rashba and atomic SOI strengths γ (left column) and Δ_{so} (right column), respectively. We use $\Delta_{so} = 19.3$ meV in the left column and $\gamma = 20$ meV in the right column. Other parameters are $\mu = -0.6$ eV, $T = 0$, $g = 0.135$ eV, $h_{x1} = 0.4$ eV, $h_{x2} = 0.1$ eV, and $n_d = 0$.

nontrivial topological excitations such as Majorana fermions [6] or skyrmions [63,64] or novel Hall phases [65]. We study the effects of the Rashba SOI and atomic SOI on the intraband and interband pairing, as shown in Fig. 2. The pairing gap Δ_a in the d_{xy} orbital is largely suppressed by the in-plane ferromagnetism, while the pairing gaps Δ_b and Δ_c in the d_{yz}, d_{zx} orbitals dominate. As depicted in Figs. 2(a) and 2(e), the pairing amplitudes Δ_b and Δ_c decrease slowly with increasing both Rashba SOI strength γ and atomic SOI strength Δ_{so} because the SOI enhances precession of electrons, leading to the slow reduction of the electron pairing. It is interesting to note that the superconductivity in the singlet interband channel and the triplet intraband and interband channels is induced by the SOI when the pairing amplitude Δ_b or Δ_c is finite, as shown in Figs. 2(b)–2(d) and 2(f)–2(h). The appearance of interband pairings can be understood from the following consideration. In the absence of the spin-orbit interactions, all three bands have parabolic dispersion with two different masses (d_{yz} and d_{zx} are degenerate), as shown in Fig. 1(a). The atomic SOI causes mixing of the bands just above the Lifshitz transition point, and the original bands effectively undergo band inversion. The Rashba SOI, on the other hand, lifts the degeneracies near the Γ point and near the points of intersection of the original bands. The pairing amplitudes in different channels are calculated in the original bands, and therefore, the finite interband pairing is nothing but the manifestation of the band-inversion phenomena arising because of the spin-orbit interactions. Due to the coexistence of the ferromagnetic spin alignment, the triplet pair with spin zero is very small in magnitude, of the order of 10^{-5}, compared

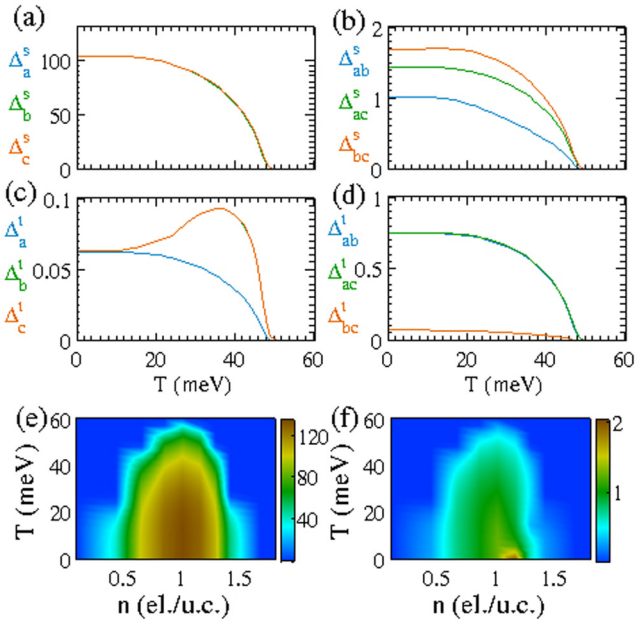

FIG. 3. (Color online) (a)–(d) The gap structures of the singlet and triplet superconductivities in intraband and interband channels. All pairing amplitudes are in meV. The maximum (e) singlet and (f) triplet pairing amplitudes plotted in the n-T plane. Other parameters are $g = 0.135$ eV, $h_{x1} = 0.4$ eV, $h_{x2} = 0.1$ eV, and $n_d = 0$.

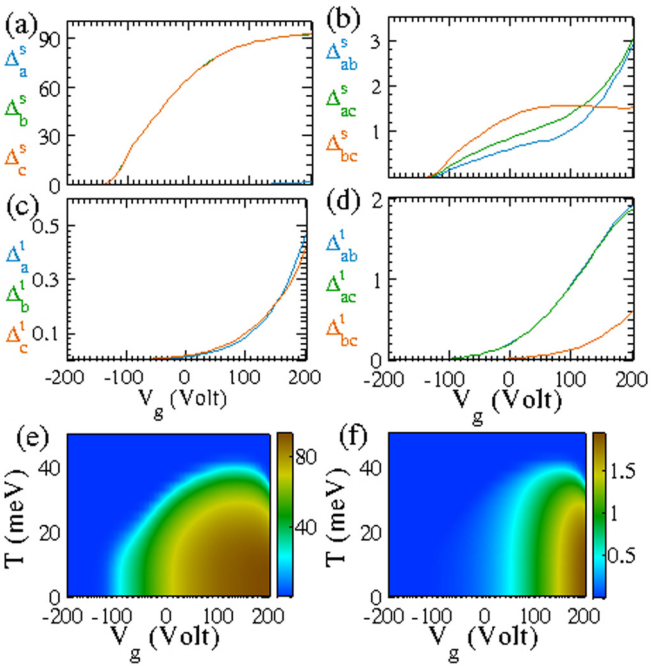

FIG. 4. (Color online) (a)–(d) Variation of the pairing amplitudes with respect to external gate voltage V_g. The maximum (e) singlet and (f) triplet pairing amplitudes plotted in the V_g-T plane. The white line in (e) indicates the experimental data, obtained from Ref. [29], showing the variation of the transition temperature T_c with V_g. Other parameters are $g = 0.135$ eV, $h_{x1} = 0.4$ eV, $h_{x2} = 0.1$ eV, and $n_d = 0$.

to the maximum pairing amplitude and is hence dropped from the analysis.

The temperature variations of the pairing amplitudes are shown in Figs. 3(a)–3(d). The pairing gaps reveal a BCS nature in all the pairing channels except the triplet intraband pairing Δ_c^t, which gets enhanced near the transition temperature. We plot the maximum pairing amplitudes in the singlet and triplet channels in the n-T phase plane as described in Figs. 3(e) and 3(f), which show the superconducting phases. It is evident that both the singlet and triplet pairing channels show a dome-shaped superconducting phase, and the triplet pairing becomes stronger towards higher values of carrier density.

In the experiments, a gate voltage V_g is tuned to control the doping level of the q2DEG, and a superconductor-to-insulator transition with a quantum critical point $V_g = 140$ V [29] is evinced by varying the gate voltage. It is therefore fascinating to study the variation of the pairing amplitudes in different channels with respect to V_g and eventually to plot the phase diagram in the V_g-T plane. In Appendix A, we derive the gate-voltage dependence of the carrier density and Rashba SOI. In Figs. 4(a)–4(d), we plot the gate-voltage variation of the pairing amplitudes, which reveals the superconducting transition at $V_g \simeq 140$ V. It is interesting to note that the singlet intraband pairing gaps and triplet intraband and interband pairing gaps follow the nature of the variation of the Rashba SOI with respect to V_g, as shown in Fig. 9(b). Figures 4(e) and 4(f) depict the superconducting phases in the singlet and triplet channels, respectively. The superconducting phase shown in Fig. 4(e) fits well with the experimental data except for a quantitative mismatch of the transition temperatures due to the inherent overestimation problem of mean-field theory. The triplet pairing appears to begin at higher values in the gate-voltage range. In the experiments, when the gate voltage is varied, the temperature T_c, at which the BKT transition takes place, shows a domelike superconducting phase in the V_g-T plane. On the other hand, the gap Δ, measured in the tunneling spectroscopic experiment, decreases in the entire gate-voltage range [52]. In subsequent tunneling spectroscopic measurements, it is revealed that Δ decreases with V_g in the underdoped regime because the phonon spectral function $\alpha^2 f(\omega)$ decreases with V_g and decreases in the overdoped regime because the additionally induced carriers do not populate the band that hosts superconductivity, and therefore, Δ is weakened by the presence of charge carriers in another band [46].

Next, we study the effect of an external in-plane magnetic field on superconductivity. As shown in Fig. 5, the magnetic field is applied in the interface plane along different directions θ with respect to the initial direction of polarization due to in-plane ferromagnetism, and the pairing gaps are plotted in the polar plane of (Δ, θ). The θ dependence of the gap components in various pairing channels exhibit sudden jumps (first order in nature) when the gap component Δ wins over the in-plane components of magnetization. The singlet components are maximized at angles in the range $\theta \simeq [90,270]$, and on the other hand, the triplet components are maximized at angles between $\theta \simeq [50,80]$ and $\theta \simeq [280,310]$. As shown in Fig. 2, the maximum singlet components (intraband or interband) appear in the upper two bands (d_{yz}/d_{zx}), in which the intrinsic magnetization is smaller ($h_{hx2} = 0.1$ eV), while the maximum triplet pairings arise in the lower band (d_{xy}), in which the

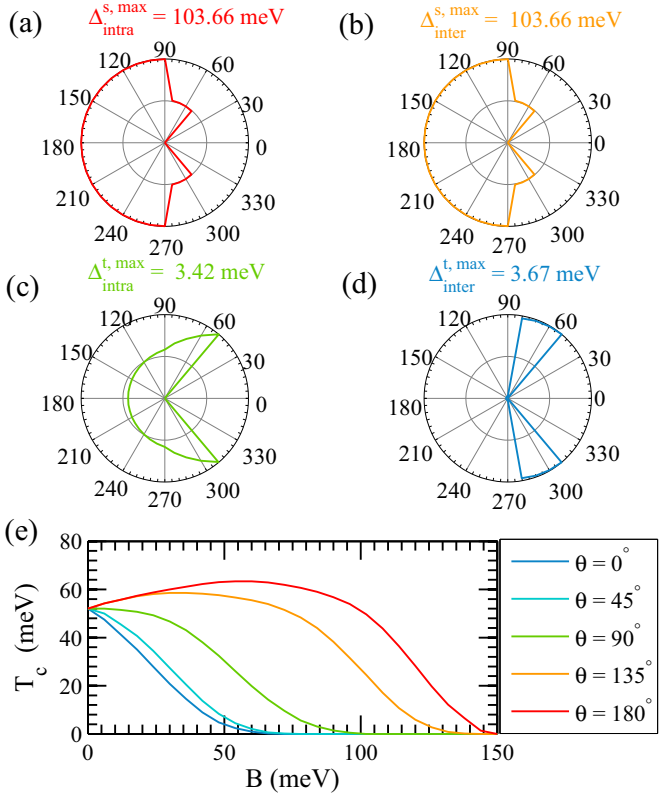

FIG. 5. (Color online) (a)–(d) Polar plots showing the angular variations of the maximum of singlet and triplet pairing amplitudes in the intraband and interband channels. The angle θ is between the initial polarization direction due to the intrinsic ferromagnetism and the applied magnetic field. (e) The variation of the superconducting transition temperature T_c with respect to the amplitude B of the magnetic field. Parameters used are $\mu = -0.6$ eV, $T = 0$ eV, $g = 0.135$ eV, $h_{x1} = 0.4$ eV, $h_{x2} = 0.1$ eV, and $n_d = 0$.

intrinsic magnetization is larger ($h_{hx1} = 0.4$ eV). Therefore, the in-plane components of magnetization are not identical in different bands, and the four pairing amplitudes in different pairing channels reveal distinct θ dependence. Figure 5(e) plots the superconducting transition temperature T_c as a function of the amplitude B of the applied magnetic field. Remarkably, the enhancement of superconductivity by in-plane magnetic field has been reported experimentally in the LAO/STO interface [53]. The enhancement of superconductivity is because of the interplay between superconductivity, the intrinsic ferromagnetism, and the ferromagnetism induced by the applied magnetic field and implicates the possibility of a hidden superconducting phase above the transition temperature. The hidden superconducting phase is also inferred from the recent observation of the magnetic-field-assisted transient superconducting state observed in the interface q2DEG at 245 mK [54]. It is relevant to mention here that a hidden order has been proposed to be the precursor of superconductivity in Fe pnictides and high-T_c cuprates [66]. It may also be possible that a hidden superconducting phase, arising from the competition between ferromagnetism and superconductivity, exists in the LAO/STO heterointerface.

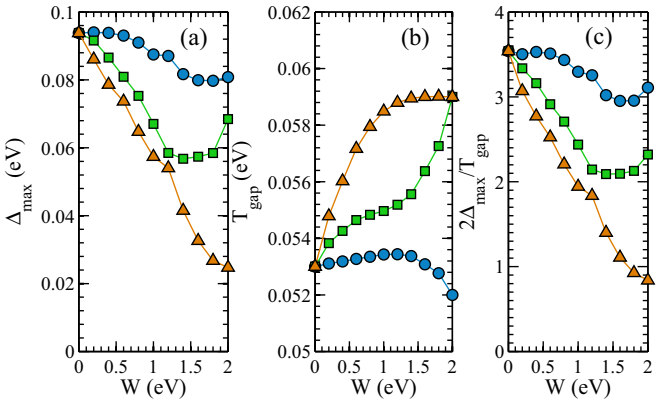

FIG. 6. (Color online) The variation of (a) the maximum pairing amplitude Δ_{max}, (b) the gap-closing temperature T_g, and (c) the BCS ratio $2\Delta_{max}/T_g$ with respect to the disorder strength W for different disorder concentrations n_d. Other parameters are $\mu = -0.6$ eV, $g = 0.135$ eV, $h_{x1} = 0.4$ eV, and $h_{x2} = 0.1$ eV.

V. MONTE CARLO STUDY OF THERMAL PHASE FLUCTUATION

The interface q2DEG is highly inhomogeneous in nature and becomes superconducting at very low carrier concentrations. Therefore, the superconductivity is prone to the detrimental effects of nonmagnetic disorder, and the role of phase fluctuation becomes important. In a previous study [4], we show that disorder, in fact, can help the antagonistic ferromagnetism to exist apart from superconductivity in spatially phase-segregated regions at the interface.

In Fig. 6, we show the variation of the maximum pairing gap Δ_{max}, the gap-closing temperature T_g, and the BCS ratio $2\Delta_{max}/T_g$ with respect to disorder strength W for different concentrations n_d. With increasing W and n_d, Δ_{max} decreases, T_g increases, and the BCS ratio deviates from its mean-field value of 3.5. It is evident that in the highly disordered limit, Δ and T_g behave differently and therefore can no longer track the superconducting transition [67]. It is necessary to go beyond the standard BCS prescription and incorporate the phase fluctuation in the effective theory. The self-consistent BdG formalism is based on mean-field treatment of the pairing interaction, and the phases of the pairing gaps are not monitored in the analysis presented previously. We use a Monte Carlo (MC) technique in conjunction with self-consistent BdG formalism to study the thermal phase- fluctuations near the superconducting transition driven by magnetic field or temperature. In the MC analysis, we consider only singlet intraband pairings in the d_{yz} and d_{zx} orbitals as they dominate over the pairings in other channels substantially and use a single pairing gap $\Delta = \Delta^s_b \simeq \Delta^s_c$ to reduce the computation time. The complex superconducting order parameter is taken as $\Delta(r_i) = |\Delta_i| e^{j\phi_i}$, where $|\Delta_i|$ and ϕ_i are, respectively, the amplitude and phase of the pairing gap at site i. We start at high temperature with a specific disorder configuration and reach low temperature up to 0.002 eV. At each temperature, the site-resolved pairing gaps $|\Delta_i|$ are computed using the self-consistent BdG method, described in Sec. III, and are fed into the MC update process, which uses a free-energy minimization technique to determine

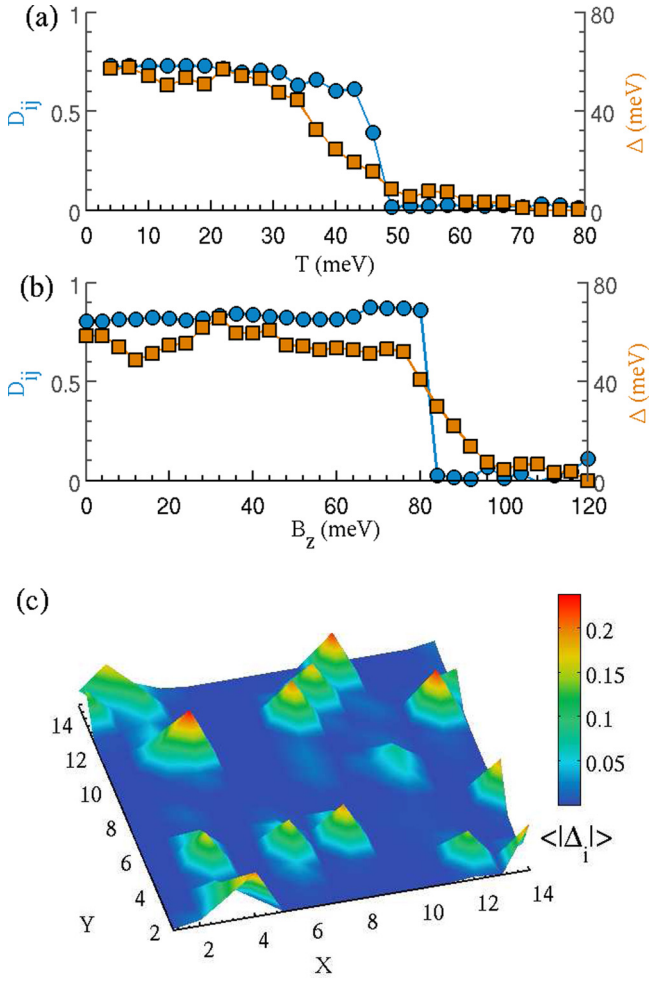

FIG. 7. (Color online) The variation of the phase correlation function D_{ij} and the disorder-averaged and site-averaged pairing amplitude $\langle|\Delta_i|\rangle$ with respect to (a) temperature T and (b) perpendicular magnetic field B_z. (c) The profile of the pairing amplitude $\langle|\Delta_i|\rangle$ at $T = 60$ meV describing the localized Cooper pairs in the nonsuperconducting side of the transition [in (a)]. A 14×14 lattice is used in the calculation. Other parameters are $\mu = -0.6$ eV, $g = 0.135$ eV, $h_{x1} = 0.4$ eV, $h_{x2} = 0.1$ eV, $W = 0.8$ eV, and $n_d = 50$.

the phases ϕ_i. In Appendix B, we present the calculation of the free energy for a given BdG Hamiltonian.

In the weak- to moderate-disorder limit, the pairing gap parameter tracks the superconducting transition. However, in the highly disordered limit, in which the interface q2DEG lies, the superconducting transition is indicated by the destruction of the global phase coherence. To quantify the phase coherence, we compute a long-ranged phase correlation function $D_{ij} = \langle\cos(\phi_i - \phi_j)\rangle$, similar to that used in the XY model to track the universal BKT transition, where i and j are sites separated by a large distance and $\langle\cdot\rangle$ denotes the disorder- and site-averaged value. In Figs. 7(a) and 7(b), we show the variation of D_{ij} and $\langle|\Delta_i|\rangle$ with respect to temperature T and perpendicular magnetic field B_z, respectively. In both the cases, the transition to the nonsuperconducting phase is dictated by a vanishing D_{ij}; on the other hand, $\langle|\Delta_i|\rangle$ remains finite and fluctuates. The small finite value of $\langle|\Delta_i|\rangle$ in the nonsuperconducting phase is the signature of localized Cooper

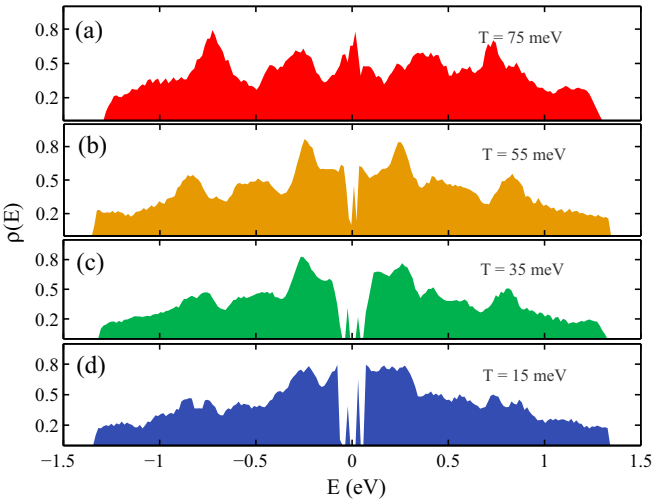

FIG. 8. (Color online) The density of states $\rho(E)$ at temperatures (a) $T = 75$ meV, (b) $T = 55$ meV, (c) $T = 35$ meV, and (d) $T = 15$ meV across the transition to the superconducting state. Parameters: are $\mu = -0.6$ eV, $g = 0.135$ eV, $h_{x1} = 0.4$ eV, $h_{x2} = 0.1$ eV, $W = 0.8$ eV, and $n_d = 50$.

pairs [68]. The profile of the pairing gap in the two-dimensional space is shown in Fig. 7(c). The direct evidence of the presence of localized Cooper pairs in the insulating phase has been found in recent transport measurement [55]. Figure 8 shows the single-particle density of states, given by

$$\rho(E) = \frac{1}{N}\sum_{n,i,\alpha,\sigma}\left[\left(u^i_{n\alpha\sigma}\right)^2\delta(E - E_n) + \left(v^i_{n\alpha\sigma}\right)^2\delta(E + E_n)\right],$$

at different temperatures across the superconducting transition. It is important to note that because of strong disorder, quasiparticle states, bound to the impurities, appear within the bulk superconducting gap, and the system passes through a pseudogaplike phase during the quantum phase transition [52].

VI. CONCLUSIONS

In this paper, we presented a three-band model for the superconductivity at the $LaAlO_3/SrTiO_3$ (001) interface. We explored, using a multiorbital BdG theory, the interplay between the superconductivity, ferromagnetism, and spin-orbit interactions. We also studied the role of thermal phase fluctuation using a Monte Carlo method. The key findings of our analysis can be summarized as follows.

The electron pairing in the d_{xy} band is suppressed by the competing ferromagnetic order, and the pairing in the d_{yz}, d_{zx} bands dominates. We find that the singlet pairing in the interband channel and the triplet pairing in both intra- and interband channels are induced by the SOI when the pairing amplitude in the singlet intraband channel is finite.

Gate voltage has been found to affect superconductivity at the interface quite strongly. We calculated the gate voltage variation of the pairing amplitudes in different channels and extracted the singlet and triplet superconducting phases in the V_g-T plane and compared the results with experimental results with a fair degree of agreement.

We observed an enhancement of superconductivity by an external in-plane magnetic field. We found that the superconducting transition temperature depends on the direction of the applied in-plane magnetic field, which is an experimentally verifiable prediction from our theory. The enhancement of superconductivity by applied magnetic field is due to the interplay between ferromagnetism and superconductivity and suggests a hidden superconducting phase above the transition temperature. The recent observation of a magnetic-field-assisted transient superconducting state at 245 mK [54] agrees with this hidden superconducting order and needs to be explored further experimentally.

Last, we studied the effect of thermal phase fluctuation on the superconductivity using a Monte Carlo method and found that there exist localized Cooper pairs in the nonsuperconducting phase beyond the quantum phase transition driven by perpendicular magnetic field. The same is also seen in the normal state just above the superconducting transition temperature. The density of states reveals that, in the highly disordered situation, quasiparticle bound states appear within the bulk superconducting gap and the system passes through a pseudogaplike phase exactly as reported in the tunneling spectroscopic measurement [52].

ACKNOWLEDGMENTS

We thank A. Bid and S. Lal for fruitful discussions and acknowledge the use of the computing facility from DST-Fund for Improvement of S&T infrastructure (phase-II) Project installed in the Department of Physics, IIT Kharagpur, India.

APPENDIX A: GATE-VOLTAGE DEPENDENCE

The voltage V_g, applied by back-gating to the STO substrate with the interface 2DEG grounded, controls the carrier density at the interface and the Rashba spin-orbit splitting [29,30]. The carrier density n changes with the applied electric field F according to the relation

$$n(F) = \frac{2\epsilon_0}{e}\int_0^F \epsilon_r(F)dF, \tag{A1}$$

where ϵ_0 is the free-space permittivity, $\epsilon_r(F)$ is the field-dependent relative permittivity, and e is the quantum of electronic charge. For bulk STO, $\epsilon_r(F) = 1/A(1 + \frac{B}{A}F)$, where $A = 4.097 \times 10^{-5}$ and $B = 4.907 \times 10^{-10}$ are temperature-dependent parameters, determined experimentally at 4.3 K by a first-order fit to the permittivity [69]. However, it has a singularity at $F = -A/B$, which is circumvented, as prescribed in Ref. [70], by taking into account the second-order term in the denominator. The corrected expression is given by $\epsilon_r(F) = 1/A[C_1 + C_2\frac{B}{A}F + C_3(\frac{B}{A})^2F^2]$, where C_i $(i = 1,2,3)$ are parameters to be found out by experimental fits. The carrier density can therefore be expressed as

$$n(F) = \frac{4\epsilon_0\left\{\tan^{-1}\left[\frac{2C_3BF+C_2A}{A\sqrt{C_4}}\right] - \tan^{-1}\left(\frac{C_2}{\sqrt{C_4}}\right)\right\}}{eB\sqrt{C_4}}, \tag{A2}$$

where $C_4 = 4C_1C_3 - C_2^2$. The gate voltage V_g enters in the above expression via the relation $F = V_g/d + F_0$, where $d = 0.5$ mm is the thickness of the STO layer and

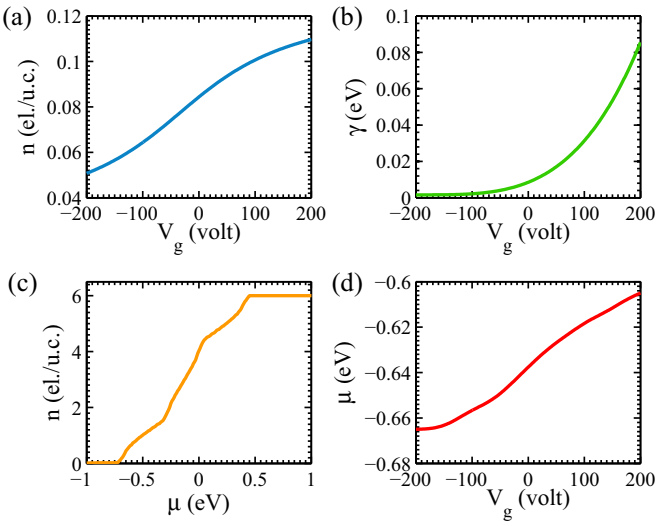

FIG. 9. (Color online) Gate voltage modulation of (a) the carrier concentration and (b) the strength of Rashba spin-orbit splitting fitted with the experimental data [29,30]. The variation of (c) the total occupation number as a function of the chemical potential and (d) the chemical potential as a function of the gate voltage at zero temperature. A carrier concentration of 10^{13} cm^{-2} is equivalent to 0.016 electrons per unit cell [71].

$F_0 = 1.2 \times 10^5$ V/m is the initial electric field at the interface in the absence of the gate voltage. Comparison with the experimental data [29] yields $C_1 = 4.25$, $C_2 = -0.37$, and $C_3 = 0.29$. Figure 9(a) describes the gate-voltage modulation of the carrier density.

Furthermore, the gate voltage tunes the Rashba spin-orbit splitting at the interface [30]. In Ref. [71], the gate-voltage dependence of the Rashba spin-orbit interaction is derived using a Kane $k \cdot p$ approach. However, it is interesting to note that the DFT studies in Ref. [39] reveal that the Rashba spin-orbit interaction at the interface is very different from the usual Rashba-type spin-orbit interaction found in semiconductor heterointerfaces. Here, we fit the gate-voltage dependence of the Rashba splitting amplitude observed in Ref. [30] to the equation $\gamma = a + b(V_g + 200)^{2c}$ within the V_g range $[-200,200]$ V, with $a = 0.0016$, $b = 3.6 \times 10^{-11}$, and $c = 1.8$, as plotted in Fig. 9(b).

APPENDIX B: FREE ENERGY OF BdG HAMILTONIAN

The free energy of an inhomogeneous superconductor is given by [72]

$$\mathcal{F} = \langle\mathcal{H}_{\text{eff}}\rangle - T\mathcal{S}, \tag{B1}$$

where $\langle\mathcal{H}_{\text{eff}}\rangle$ is the effective Hamiltonian of the superconductor, T is the temperature, and $\mathcal{S}$ is the entropy.

The effective mean-field Hamiltonian of a single-orbital system is written as

$$\mathcal{H}_{\text{eff}} = \sum_{ij,\sigma} H_{ij}c^\dagger_{i\sigma}c_{i\sigma} + \sum_i[\Delta_i c^\dagger_{i\uparrow}c^\dagger_{i\downarrow} + \text{H.c.}] + \frac{|\Delta_i|^2}{U}, \tag{B2}$$

where H_{ij} is the tight-binding Hamiltonian containing kinetic-energy terms, Δ_i is the complex superconducting pairing gap at site i, and U is the strength of the attractive electron-electron interaction.

The effective Hamiltonian $\mathcal{H}_{\rm eff}$ is diagonalized by using the Bogoliubov transformation $\hat{c}_{i\sigma} = \sum_{n,\sigma'} u^i_{n\sigma\sigma'}\hat{\gamma}_{n\sigma'} + v^{i*}_{n\sigma\sigma'}\hat{\gamma}^\dagger_{n\sigma'}$ to obtain

$$\mathcal{H}_{\rm eff} = E_g + \sum_n E_n \gamma^\dagger_{n\sigma'}\gamma_{n\sigma'}, \tag{B3}$$

where E_n are the eigenvalues of the BdG equations and the ground-state energy E_g is given by

$$E_g = -\sum_{i,n,\sigma} E_n \left|v^i_{n\sigma}\right|^2 + \sum_i \frac{|\Delta_i|^2}{U}. \tag{B4}$$

The entropy of an ideal gas of fermionic quasiparticles is expressed as [73]

$$\mathcal{S} = -\sum_n [f_n \ln f_n + (1-f_n)\ln(1-f_n)]. \tag{B5}$$

Therefore, using $\langle\gamma^\dagger_{n\sigma'}\gamma_{n\sigma'}\rangle = f_{n\sigma'}$ and $f_{n\uparrow} = f_{n\downarrow} = f_n$, Eq. (B1) becomes

$$\mathcal{F} = -\sum_{i,n,\sigma} E_n \left|v^i_{n\sigma}\right|^2 + \sum_i \frac{|\Delta_i|^2}{U} + \sum_n E_n f_n + T\sum_n [f_n \ln f_n + (1-f_n)\ln(1-f_n)]. \tag{B6}$$

Evidently, the free energy can be calculated if the solution of the BdG Hamiltonian is known.

[1] N. Reyren, S. Thiel, A. D. Caviglia, L. F. Kourkoutis, G. Hammerl, C. Richter, C. W. Schneider, T. Kopp, A.-S. Retschi, D. Jaccard, M. Gabay, D. A. Muller, J.-M. Triscone, and J. Mannhart, Science **317**, 1196 (2007).

[2] S. Gariglio, N. Reyren, A. D. Caviglia, and J.-M. Triscone, J. Phys. Condens. Matter **21**, 164213 (2009).

[3] K. Michaeli, A. C. Potter, and P. A. Lee, Phys. Rev. Lett. **108**, 117003 (2012).

[4] N. Mohanta and A. Taraphder, J. Phys. Condens. Matter **26**, 025705 (2014).

[5] N. Mohanta and A. Taraphder, J. Phys. Condens. Matter **26**, 215703 (2014).

[6] N. Mohanta and A. Taraphder, Europhys. Lett. **108**, 60001 (2014).

[7] S. Caprara, J. Biscaras, N. Bergeal, D. Bucheli, S. Hurand, C. Feuillet-Palma, A. Rastogi, R. C. Budhani, J. Lesueur, and M. Grilli, Phys. Rev. B **88**, 020504 (2013).

[8] N. Ganguli and P. J. Kelly, Phys. Rev. Lett. **113**, 127201 (2014).

[9] N. Pavlenko, Phys. Rev. B **80**, 075105 (2009).

[10] M. Stengel and D. Vanderbilt, Phys. Rev. B **80**, 241103 (2009).

[11] S. N. Klimin, J. Tempere, J. T. Devreese, and D. van der Marel, Phys. Rev. B **89**, 184514 (2014).

[12] L. Fidkowski, H.-C. Jiang, R. M. Lutchyn, and C. Nayak, Phys. Rev. B **87**, 014436 (2013).

[13] S. B. Chung, C. Chan, and H. Yao, arXiv:1505.00790.

[14] L. Li, C. Richter, J. Mannhart, and R. C. Ashoori, Nat. Phys. **7**, 762 (2011).

[15] D. A. Dikin, M. Mehta, C. W. Bark, C. M. Folkman, C. B. Eom, and V. Chandrasekhar, Phys. Rev. Lett. **107**, 056802 (2011).

[16] A. Ron, E. Maniv, D. Graf, J.-H. Park, and Y. Dagan, Phys. Rev. Lett. **113**, 216801 (2014).

[17] M. H. Fischer, S. Raghu, and E.-A. Kim, New J. Phys. **15**, 023022 (2013).

[18] A. Fête, S. Gariglio, A. D. Caviglia, J.-M. Triscone, and M. Gabay, Phys. Rev. B **86**, 201105 (2012).

[19] Z. Q. Liu, C. J. Li, W. M. Lü, X. H. Huang, Z. Huang, S. W. Zeng, X. P. Qiu, L. S. Huang, A. Annadi, J. S. Chen, J. M. D. Coey, T. Venkatesan, and Ariando, Phys. Rev. X **3**, 021010 (2013).

[20] Y. Li, S. N. Phattalung, S. Limpijumnong, J. Kim, and J. Yu, Phys. Rev. B **84**, 245307 (2011).

[21] Z. Zhong, P. X. Xu, and P. J. Kelly, Phys. Rev. B **82**, 165127 (2010).

[22] A. Ohtomo and H. Y. Hwang, Nature (London) **427**, 423 (2004).

[23] S. Thiel, G. Hammerl, A. Schmehl, C. W. Schneider, and J. Mannhart, Science **313**, 1942 (2006).

[24] M. Huijben, G. Rijnders, D. H. A. Blank, S. Bals, S. V. Aert, J. Verbeeck, G. V. Tendeloo, A. Brinkman, and H. Hilgenkamp, Nat. Mater. **5**, 556 (2006).

[25] C. Cen, S. Thiel, G. Hammerl, C. W. Schneider, K. E. Andersen, C. S. Hellberg, J. Mannhart, and J. Levy, Nat. Mater. **7**, 298 (2008).

[26] G. Rijnders and D. H. A. Blank, Nat. Mater. **7**, 270 (2008).

[27] F. Cossu, U. Schwingenschlögl, and V. Eyert, Phys. Rev. B **88**, 045119 (2013).

[28] V. T. Tra, J.-W. Chen, P.-C. Huang, B.-C. Huang, Y. Cao, C.-H. Yeh, H.-J. Liu, E. A. Eliseev, A. N. Morozovska, J.-Y. Lin, Y.-C. Chen, M.-W. Chu, P.-W. Chiu, Y.-P. Chiu, L.-Q. Chen, C.-L. Wu, and Y.-H. Chu, Adv. Mater. **25**, 3357 (2013).

[29] A. D. Caviglia, S. Gariglio, N. Reyren, D. Jaccard, T. Schneider, M. Gabay, S. Thiel, G. Hammerl, J. Mannhart, and J.-M. Triscone, Nature (London) **456**, 624 (2008).

[30] A. D. Caviglia, M. Gabay, S. Gariglio, N. Reyren, C. Cancellieri, and J.-M. Triscone, Phys. Rev. Lett. **104**, 126803 (2010).

[31] J. Mannhart and D. G. Schlom, Science **327**, 1607 (2010).

[32] L. Bjaalie, B. Himmetoglu, L. Weston, A. Janotti, and C. G. V. de Walle, New J. Phys. **16**, 025005 (2014).

[33] N. Nakagawa, H. Y. Hwang, and D. A. Muller, Nat. Mater. **5**, 204 (2006).

[34] Z. S. Popović, S. Satpathy, and R. M. Martin, Phys. Rev. Lett. **101**, 256801 (2008).

[35] N. Pavlenko, T. Kopp, E. Y. Tsymbal, G. A. Sawatzky, and J. Mannhart, Phys. Rev. B **85**, 020407 (2012).

[36] R. Pentcheva and W. E. Pickett, Phys. Rev. B **74**, 035112 (2006).

[37] P. Delugas, A. Filippetti, V. Fiorentini, D. I. Bilc, D. Fontaine, and P. Ghosez, Phys. Rev. Lett. **106**, 166807 (2011).

[38] M. Hirayama, T. Miyake, and M. Imada, J. Phys. Soc. Jpn. **81**, 084708 (2012).

[39] Z. Zhong, A. Tóth, and K. Held, Phys. Rev. B **87**, 161102 (2013).

[40] G. Khalsa, B. Lee, and A. H. MacDonald, Phys. Rev. B **88**, 041302 (2013).

[41] M. Ben Shalom, M. Sachs, D. Rakhmilevitch, A. Palevski, and Y. Dagan, Phys. Rev. Lett. **104**, 126802 (2010).
[42] A. Joshua, J. Ruhman, S. Pecker, E. Altman, and S. Ilani, Proc. Natl. Acad. Sci. U.S.A. **110**, 9633 (2013).
[43] A. Joshua, S. Pecker, J. Ruhman, E. Altman, and S. Ilani, Nat. Commun. **3**, 1129 (2012).
[44] J. A. Bert, B. Kalisky, C. Bell, M. Kim, Y. Hikita, H. Y. Hwang, and K. A. Moler, Nat. Phys. **7**, 767 (2011).
[45] M. S. Scheurer and J. Schmalian, Nat. Commun. **6**, 6005 (2015).
[46] H. Boschker, C. Richter, E. Fillis-Tsirakis, C. W. Schneider, and J. Mannhart, Sci. Rep. **5**, 12309 (2015).
[47] C. S. Koonce, M. L. Cohen, J. F. Schooley, W. R. Hosler, and E. R. Pfeiffer, Phys. Rev. **163**, 380 (1967).
[48] J. F. Schooley, W. R. Hosler, and M. L. Cohen, Phys. Rev. Lett. **12**, 474 (1964).
[49] J. Biscaras, N. Bergeal, A. Kushwaha, T. Wolf, A. Rastogi, R. C. Budhani, and J. Lesueur, Nat. Commun. **1**, 89 (2010).
[50] P. Moetakef, J. R. Williams, D. G. Ouellette, A. P. Kajdos, D. Goldhaber-Gordon, S. J. Allen, and S. Stemmer, Phys. Rev. X **2**, 021014 (2012).
[51] J. J. Lee, F. T. Schmitt, R. G. Moore, S. Johnston, Y.-T. Cui, W. Li, M. Yi, Z. K. Liu, M. Hashimoto, Y. Zhang, D. H. Lu, T. P. Devereaux, D.-H. Lee, and Z.-X. Shen, Nature (London) **515**, 245 (2014).
[52] C. Richter, H. Boschker, W. Dietsche, E. Fillis-Tsirakis, R. Jany, F. Loder, L. F. Kourkoutis, D. A. Muller, J. R. Kirtley, C. W. Schneider, and J. Mannhart, Nature (London) **502**, 528 (2013).
[53] H. J. Gardner, A. Kumar, L. Yu, P. Xiong, M. P. Warusawithana, L. Wang, O. Vafek, and D. G. Schlom, Nat. Phys. **7**, 895 (2011).
[54] S. Kumar, G. Nath Daptary, P. Kumar, A. Dogra, N. Mohanta, A. Taraphder, R. C. Budhani, and A. Bid, arXiv:1411.3103.
[55] M. Mehta, D. Dikin, C. Bark, S. Ryu, C. Folkman, C. Eom, and V. Chandrasekhar, Nat. Commun. **3**, 955 (2012).
[56] S. Banerjee, O. Erten, and M. Randeria, Nat. Phys. **9**, 626 (2013).
[57] J.-S. Lee, Y. W. Xie, H. K. Sato, C. Bell, Y. Hikita, H. Y. Hwang, and C.-C. Kao, Nat. Mater. **12**, 703 (2013).
[58] J. Zhou, W.-Y. Shan, and D. Xiao, Phys. Rev. B **91**, 241302 (2015).
[59] Y. Nakamura and Y. Yanase, J. Phys. Soc. Jpn. **82**, 083705 (2013).
[60] M. Kim, Y. Kozuka, C. Bell, Y. Hikita, and H. Y. Hwang, Phys. Rev. B **86**, 085121 (2012).
[61] K. K. Ng and M. Sigrist, Europhys. Lett. **49**, 473 (2000).
[62] M. Bibes, N. Reyren, E. Lesne, J.-M. George, C. Deranlot, S. Collin, A. Barthélémy, and H. Jaffrès, Philos. Trans. R. Soc. A **370**, 4958 (2012).
[63] X. Li, W. V. Liu, and L. Balents, Phys. Rev. Lett. **112**, 067202 (2014).
[64] D. F. Agterberg, E. Babaev, and J. Garaud, Phys. Rev. B **90**, 064509 (2014).
[65] N. Mohanta, S. Bandopadhyay, S. Lal, and A. Taraphder, arXiv:1407.6539.
[66] A. Moor, A. F. Volkov, and K. B. Efetov, Phys. Rev. B **91**, 064511 (2015).
[67] A. Ghosal, M. Randeria, and N. Trivedi, Phys. Rev. B **65**, 014501 (2001).
[68] Y. Dubi, Y. Meir, and Y. Avishai, Nature (London) **449**, 876 (2007).
[69] R. Neville, B. Hoeneisen, and C. A. Mead, J. Appl. Phys. **43**, 3903 (1972).
[70] J. T. Haraldsen, P. Wölfle, and A. V. Balatsky, Phys. Rev. B **85**, 134501 (2012).
[71] D. Bucheli, M. Grilli, F. Peronaci, G. Seibold, and S. Caprara, Phys. Rev. B **89**, 195448 (2014).
[72] I. Kosztin, Š. Kos, M. Stone, and A. J. Leggett, Phys. Rev. B **58**, 9365 (1998).
[73] L. D. Landau and E. M. Lifshitz, *Theoretical Physics*, Vol. 5, *Statistical Physics*, 3rd ed. (Pergamon, Oxford, 1980).